Early Local Last Glacial Maximum in the Tropical Andes

Jacqueline A. Smith,[1]* Geoffrey O. Seltzer,[1]† Daniel L. Farber,[2] Donald T. Rodbell,[3] Robert C. Finkel[4]

The local last glacial maximum in the tropical Andes was earlier and less extensive than previously thought, based on 106 cosmogenic ages (from beryllium-10 dating) from moraines in Peru and Bolivia. Glaciers reached their greatest extent in the last glacial cycle ~34,000 years before the present and were retreating by ~21,000 years before the present, implying that tropical controls on ice volumes were asynchronous with those in the Northern Hemisphere. Our estimates of snowline depression reflect about half the temperature change indicated by previous widely cited figures, which helps resolve the discrepancy between estimates of terrestrial and marine temperature depression during the last glacial cycle.

It is unclear whether the last glacial maximum (LGM) was a globally synchronous event or whether a local last glacial maximum (LLGM) occurred in the tropics at a different time (*1*). This issue has broad implications for our understanding of the forcings that underlie the massive global climate changes associated with glacial cycles, and it underpins all paleoclimate reconstructions for the tropics. An absolute chronology for the last glacial cycle and ice coverage in the tropics is unavailable, largely because of the limitations of radiocarbon dating and the scarcity of datable material in glacial environments above 4000 m above sea level (masl). Existing glacial chronologies for the tropics are based primarily on minimum-limiting radiocarbon dates and relative dating techniques (*2*). An absolute chronology would have important implications for paleoclimate reconstructions and the debates over the synchroneity of glaciation in the Northern and Southern Hemispheres (*3*), the synchroneity of continental and mountain glaciation (*4*), the magnitude of tropical climate change at the LGM (*5*–*7*), and the relation between sea surface temperatures (SSTs) and temperatures over continental regions (*8*). Snowline depression of ~1000 m at a presumed LGM age of ~21 thousand years before the present (ky B.P.) is often cited as evidence for terrestrial temperatures 5° to 6°C cooler than at present in the tropics (*6*). However, the climatic interpretation of snowline depression is complicated (*9*), because the timing of glacial coverage in the tropics has been poorly constrained. Here we present an absolute chronology of the LLGM based on cosmogenic dating (^{10}Be) of erratics on moraines in the tropical Andes of Peru and Bolivia.

We selected field areas that allowed direct comparison of our terrestrial glacial chronology to existing lacustrine paleoclimate records from nearby lakes: Lake Junin (11°S, 76°W) in central Peru and Lake Titicaca (16°S, 69°W) on the Peruvian-Bolivian Altiplano (Fig. 1). Both lakes predate the last glacial-interglacial transition and have provided valuable paleoclimate proxy records in the form of sediment cores (*10*–*14*). Lake Junin and Lake Titicaca lie on high plateaus (>3800 masl) between the eastern and western cordillera of the Andes and receive moisture predominantly from easterly winds crossing the Amazon Basin during the austral summer (*15*). We dated moraines in four valleys in the eastern cordillera bordering Lake Junin and in Milluni and Zongo Valleys in the Cordillera Real, approximately 35 km east of Lake Titicaca (fig. S1 and supporting online text). We used the concentration of cosmogenic ^{10}Be to determine the exposure ages of boulders on moraines in the study areas (Table 1 and table S1) (*16*, *17*). Analytical uncertainties on the entire set of exposure ages average 3.0 ± 1.5% (*17*). We assigned dated moraines to one of four moraine groups (A to D) based on an assessment of the position of the moraine within the valley, the geomorphic character of the moraine, and the exposure ages obtained from the moraine.

In the Junin valleys (Fig. 2A and fig. S1, A to D), 146 ^{10}Be exposure ages clearly distinguish moraines deposited late in the last glacial cycle from moraines that are considerably older (Fig. 3). Exposure ages of boulders on LLGM moraines are typically 34 to 22 ky B.P.; ages on older moraines generally predate the last glacial cycle (>65 ky B.P.) and in many cases are dated >200 ky B.P. (*18*). In the west-facing valleys, the LLGM moraine is the lower of two end moraines that are located midway downvalley; a younger (~20 to 16 ky B.P.) moraine typically dams a lake (or paleolake) 1 to 2 km upvalley from the LLGM ice limit.

In the Cordillera Real (Fig. 2B and fig. S1, E and F), all 42 of the ^{10}Be exposure ages fall within the last glacial cycle (table S1). In Milluni Valley, exposure ages on two sharp-crested parallel lateral moraines sampled at ~4500 to 4600 masl lie between 34 and 23 ky B.P. (with two younger outliers). Exposure ages on a recessional moraine at ~4650 masl are late glacial to early Holocene (18 to 9 ky B.P.). All exposure ages from Zongo Valley, even those from the lateral moraines at 3400 to 3500 masl, are late glacial (<20 ka) or younger (*19*).

The pattern of LLGM moraine ages in the Junin region is consistent from valley to valley, whereas the pattern in the Cordillera Real is not. Exposure ages in the Junin region suggest that glaciers reached their maximum extent of the last glacial cycle as early as ~34 ky B.P. Recession was under way by ~21 ky B.P., followed by stillstand or readvance

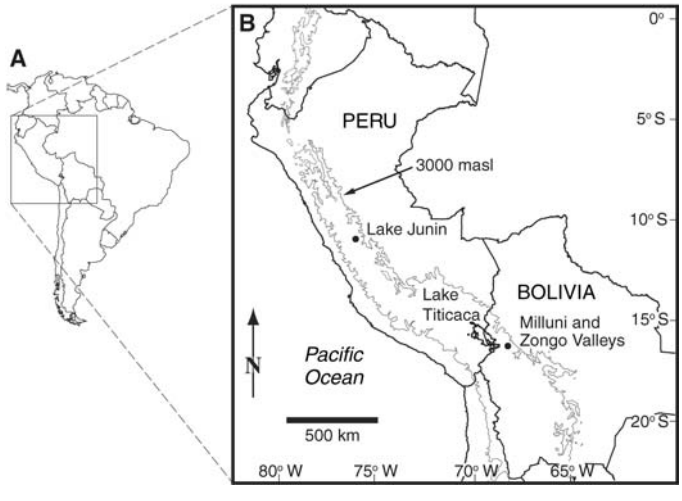

Fig. 1. Site location maps of the study areas. (**A**) South America, with area covered by (**B**) indicated. (**B**) Map of Peru, Bolivia, and adjacent countries, showing the general location of Lake Junin and the Junin valleys, Lake Titicaca, and Milluni and Zongo Valleys in the Cordillera Real. The 3000-m contour line bounds the eastern and western cordillera of the Andes and the intervening high plateaus, including the Altiplano.

[1]204 Heroy Geology Laboratory, Department of Earth Sciences, Syracuse University, Syracuse, NY 13244–1070, USA. [2]Lawrence Livermore National Laboratory, Post Office Box 808, L-201, Livermore, CA 94551, USA. [3]Department of Geology, Olin Building, Union College, Schenectady, NY 12308, USA. [4]Center for Accelerator Mass Spectrometry, MS L-397, Lawrence Livermore National Laboratory, 7000 East Avenue, Livermore, CA 94550–9234, USA.

*To whom correspondence should be addressed. E-mail: jasmit10@syr.edu
†Deceased.

between ~16 and 20 ky B.P. In Milluni Valley, the maximum extent of ice during the last glacial cycle occurred ~34 to 23 ky B.P., with subsequent recession and several stillstands or readvances (*20*). In Zongo Valley, however, late-glacial ice extended downvalley more than 1 km lower in altitude than ice of similar age in Milluni Valley. We have not yet identified a moraine older than 20 ky B.P. in Zongo Valley. If the LLGM terminus descended past 3400 masl to ~3000 masl, as seems likely from geomorphic evidence, Müller's (*21*) estimate of ~4100 to 4200 masl for the LLGM limit was too high by at least 700 m and perhaps by more than 1 km.

Our glacial chronology is consistent with the paleoclimate proxy records from Lake Junin and Lake Titicaca. Seltzer *et al.* (*10*, *11*) used magnetic susceptibility (MS) and stratigraphic records to bracket the LLGM between ~30 ky B.P. and ~21 ky B.P. in a sediment core from Lake Junin with a basal age of ~40 ^{14}C ky B.P. (radiocarbon years before the present). MS in Lake Junin sediments was elevated (relative to Holocene and late-glacial levels) even before 30 ky B.P., including sharp increases ~37 to 35 and ~33 ky B.P. (*10*, *11*). Seltzer *et al.* (*10*) identified the glacial-interglacial transition with a dramatic drop in MS ~21 ky B.P. and the onset of full deglaciation with the increase in organic carbon ~16 ky B.P. Our record from the Junin valleys suggests maximum ice extent ~34 to 22 ky B.P., ice retreat from the terminal moraine by 21 ky B.P., formation of a second end moraine upvalley between ~20 and 16 ky B.P., and steady retreat after ~15 ky B.P. Lake Titicaca sediment cores indicate a wet glacial period and the onset of deglaciation ~24 to 19 ky B.P. The LGM and late-glacial period (until ~15 ky B.P.) on the Altiplano were wet (*12*, *13*) and lake levels were high (*14*). Temperature decreased by ~5°C from 27.5 to 21 ky B.P. and warming began ~21 ky B.P. (*14*). Seltzer *et al.* (*11*) identified the glacial-interglacial transition with decreases in MS and sedimentation rates ~24 and ~19.5 ky B.P., respectively, in two sediment cores from Lake Titicaca that show elevated MS before the transition. Our glacial chronology shows maximum ice extent in Milluni Valley ~34 to 23 ky B.P. and construction of a recessional moraine (~10 km upvalley and ~50 m higher in altitude) by 18 ky B.P. Exposure ages suggest that ice remained in Zongo Valley almost into the Holocene.

We estimate that equilibrium-line altitude (ELA) depression at the LLGM was 300 to 600 m in the Junin valleys and Milluni Valley and 800 to 1000 m in Zongo Valley (fig. S2). Even with uncertainty of ±100 m, our estimates of LLGM ELA depression for the Junin valleys and Milluni Valley are about half of published estimates of 900 to 1000 m for the tropical Andes (*6*, *7*). We can use the position of LLGM moraines to constrain paleoclimatic change at the time of moraine deposition. If we assume that the change in ELA (ΔELA) was entirely a function of a change in temperature (ΔT), we estimate a ΔT of –2° to –4°C in the Junin valleys and Milluni Valley at the LLGM [using a moist adiabatic lapse rate of 6°C/km (*7*)]. Recent estimates put the LLGM temperature depression in the tropical Andes and Amazon Basin at ~5°C (*14*, *22*) and the change in SST in the eastern equatorial Pacific at –2.8° ± 0.7°C (*23*). If the Junin and Milluni estimates of ΔELA accurately reflect the ΔT at the LLGM, as these recent ΔT estimates suggest, then we can infer that the Zongo Valley glacier was anomalously long.

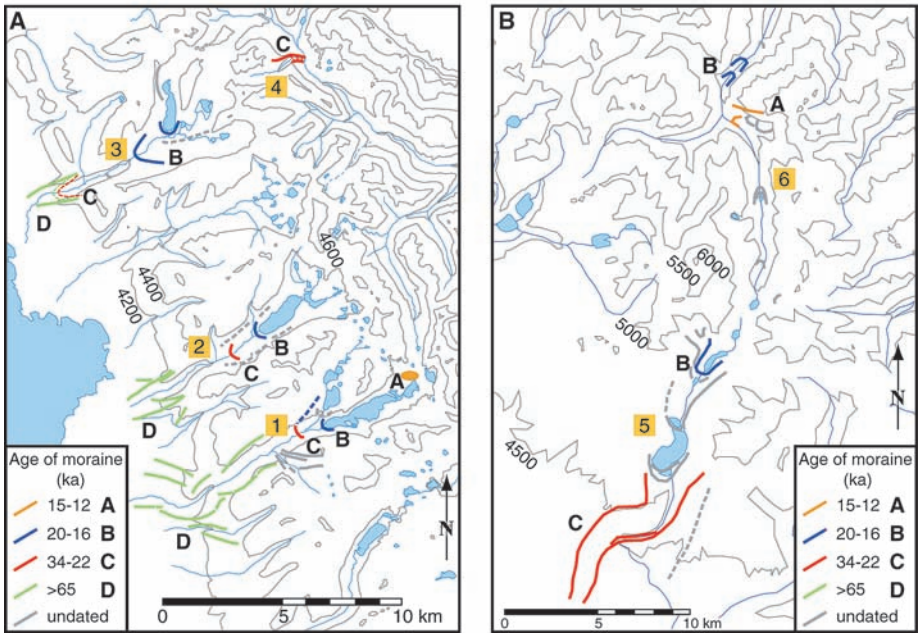

Fig. 2. Exposure ages of moraines in the Junin valleys (**A**) and Milluni and Zongo Valleys (**B**) based on cosmogenic dating with ^{10}Be. Thin gray lines are contour lines, with altitudes in masl; contour intervals are 200 m (A) and 500 m (B). Heavier solid lines indicate distinct moraines observed in the field and/or on aerial photographs; dashed lines indicate less distinct moraines or boulder trains. Ages shown were calculated without erosion or uplift (*17*). Analytical uncertainties on exposure ages average 3.0 ± 1.5% for all moraine groups combined (moraine groups A, B, C, and D). The LLGM in both areas was reached ~34 ky B.P. (A) The Junin valleys include Alcacocha Valley (1), Antacocha Valley (2), Calcalcocha Valley (3), and Collpa Valley (4). In west-facing Junin valleys, LLGM glaciers (moraine group C) were small relative to glaciers that deposited larger moraines downvalley (moraine group D) before the last glacial cycle (≫65 ky B.P.). (B) In Milluni Valley (5) and Zongo Valley (6), all moraines that we have dated were deposited during the last glacial cycle (<65 ky B.P.). Contemporaneous moraines lie more than 1000 m lower in Zongo Valley than in Milluni Valley. Detailed sampling locations are illustrated in fig. S1.

Table 1. Exposure ages (^{10}Be) for moraine groups A to C deposited during the last glacial cycle (*17*). Statistical data are shown for sample ages excluding outliers (I) and for all sample ages (II). As used here, the term "outliers" refers to exposure ages greater than 2 standard deviations (SD) from the mean age of the moraine group.

Moraine group	(I) Mean age (excluding outliers) (years)	SD of the ages (excluding outliers) (years)	Age range (excluding outliers) (years)	(II) Mean age (all samples) (years)	SD of the ages (all samples) (years)	Age range (all samples) (years)	Number of samples (including outliers)	Number of outliers (>2σ from mean)	Relative SD*	Analytical uncertainty†
A	14,500	2,000	11,500–18,400	15,300	4,300	11,500–31,100	19	1	14%	4.1%
B	16,300	2,900	7,900–22,700	15,900	4,400	3,500–29,700	50	4	18%	4.2%
C	27,800	6,400	15,500–53,200	32,100	27,200	15,500–189,900	37	1	17%	3.2%

*Relative SD = (SD of the ages, excluding outliers)/(mean ^{10}Be age, excluding outliers). †Analytical uncertainty is the blank-corrected uncertainty in the accelerator mass spectrometer measurements.

The length of the Zongo Valley glacier can be explained by the effects of local factors such as shading by the sheer valley walls (*24*) and debris cover on the ice surface (*25*), compounded by orographically controlled precipitation resulting from moisture-bearing easterlies (*26*) and/or the positive feedback set up by ice advancing into a steep, positive precipitation gradient. Thus, our findings sound a note of caution for the use of generalized ELA estimates in paleoclimate reconstructions for areas of complex topography such as the Andes.

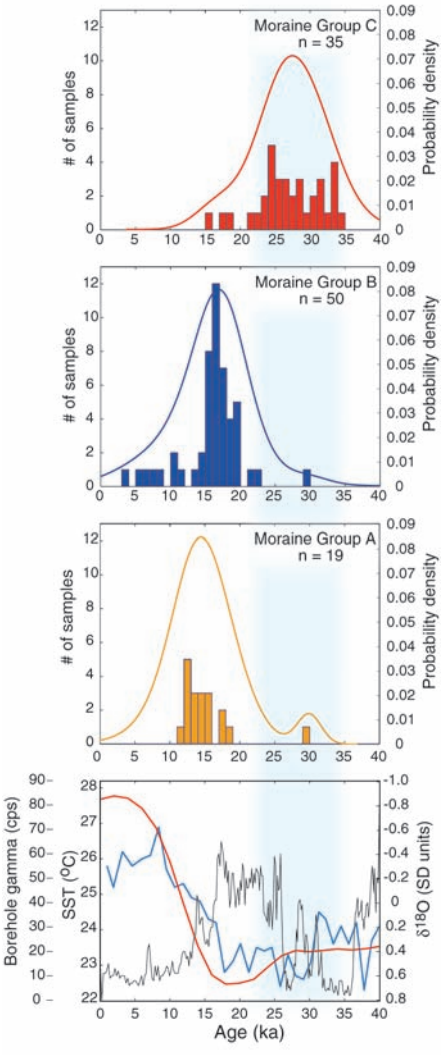

Fig. 3. Exposure ages and paleoclimate proxy records for 0 to 40 ky B.P. The top three panels are histograms and probability density (PD) curves (*32*) showing age distributions for cosmogenic ^{10}Be exposure ages in moraine groups C, B, and A, respectively, from the top down; *n* refers to the number of samples included in the histogram and PD curves. Analytical uncertainties on exposure ages average 3.8 ± 1.4% for moraine groups A, B, and C combined (moraine group D is omitted). Two exposure ages >40 ky B.P. have been omitted from the histogram for moraine group C (see table S1). The bottom panel shows borehole gamma radiation readings [in counts per second (cps)] from the Salar de Uyuni, Bolivia [outer left *y* axis, black curve (*27*)], SSTs at the Cocos Ridge reconstructed from Mg/Ca ratios in foraminifer shells from core TR163-19 [inner left *y* axis, blue curve (*23*)], and the SPECMAP stacked benthic δ^{18}O record [right *y* axis, red curve (*29*)]. Higher borehole gamma readings are interpreted as indicating wetter conditions (*27*), and higher (positive) benthic δ^{18}O values are interpreted as indicating greater global ice volume (*29*). The vertical blue band spanning the four panels marks the LLGM in the tropical Andes.

We propose that a shifting balance between temperature and precipitation changes promoted glacier development and expansion early in the last glacial cycle and that warming initiated deglaciation ~21 ky B.P. The SST record from the Cocos Ridge in the eastern equatorial Pacific (Fig. 3) shows overall lower SSTs from ~70 to 12 ky B.P., with sharp decreases at ~68 to 65 ky B.P., ~38 ky B.P., ~30 to 25 ky B.P., and ~22 to 16 ky B.P. (*23*). Published moisture records suggest that the last glacial cycle was wetter than the present (*27*, *28*). A moisture record for the Salar de Uyuni (~20°S) on the southern Bolivian Altiplano (*27*) indicates a dry period from ~67 to 61 ky B.P., followed by wetter conditions with periods of perennial lakes from ~60 to 15 ky B.P., and finally dry conditions from ~15 ky B.P. to the present. Ice may have begun to accumulate in the highest areas as soon as precipitation increased at ~60 ky B.P. and then expanded after the sharp SST cooling at ~38 ky B.P. (*23*). With increased precipitation and persistent cool temperatures, glaciers in the highest areas reached their maxima at ~34 ky B.P., while ice began to accumulate and/or expand in the broader Junin valleys with lower headwalls. Glaciers retreated behind their end moraines at ~22 to 21 ky B.P. in response to warming. Glaciers stabilized at their new positions for ~5000 years, from ~20 to 16 ky B.P.; the resulting recessional moraines dam lakes (or paleolakes) in the west-facing Junin valleys (fig. S1). The scarcity of younger moraines upvalley from these lakes indicates that the subsequent and final deglaciation was steady, leaving the basins relatively free of fluvioglacial deposits and till. Decreasing precipitation (driven by the precession cycle) and further warming after ~15 ky B.P. made this last deglaciation a rapid one. However, in steep and deep valleys on the eastern side of the eastern cordillera, such as Zongo Valley, deglaciation proceeded differently. There, the combination of sheer valley walls that shaded the glacier; rockfall and erosional debris that insulated the ice; and orographically controlled precipitation that supplied the accumulation area maintained the glacier terminus at an altitude more than 1 km lower than those of contemporaneous termini of paleoglaciers on the western side (fig. S1).

Our results indicate that the LLGM in the tropical Andes began ~34 ky B.P., thus preceding by as much as ~10 to 12 ky B.P. the maximum continental ice volume of the last glacial cycle as inferred from the marine oxygen isotope record (*29*). We estimate that ELA depression was typically about half the widely cited value of ~900 to 1000 m, except where local factors enhanced glacier size. The close agreement between our ^{10}Be-derived chronology and paleoclimate proxy records from nearby lakes shows that these tropical mountain glaciers are sensitive indicators of tropical climate that integrate a combination of climatic variables into a seemingly simple signal. The mountain glaciers of the tropical Andes apparently reached their maximum extent of the last glacial cycle before the continental ice sheets (Fig. 3) (*29*). Records of mountain glaciations from some other mid- and high-latitude regions have shown similar divergence from global ice volume records (*29*–*31*), thus reflecting a complex mosaic of regional climatic patterns during the last glacial cycle.

The asynchroneity in timing of the LLGM in the tropics and ice extent in the Northern Hemisphere implies that the climate-forcing mechanisms were decoupled at some level during the last glacial cycle. This, in turn, challenges conclusions about interhemispheric teleconnections that are based on the assumption that the LGM was globally synchronous (*3*) and that the magnitude of mountain snowline depression was uniform everywhere.

References and Notes

1. G. O. Seltzer, *Quat. Sci. Rev.* **20**, 1063 (2001).
2. J. A. Smith, G. O. Seltzer, D. T. Rodbell, A. G. Klein, *Quat. Int.*, in press.
3. P. U. Clark, R. B. Alley, D. Pollard, *Science* **286**, 1104 (1999).
4. A. Gillespie, P. Molnar, *Rev. Geophys.* **33**, 311 (1995).
5. CLIMAP, *Geol. Soc. Am. Map Chart Ser.* **MC-36** (1981).
6. S. C. Porter, *Quat. Sci. Rev.* **20**, 1067 (2001).
7. A. G. Klein, G. O. Seltzer, B. L. Isacks, *Quat. Sci. Rev.* **18**, 63 (1999).
8. D. Rind, D. Peteet, *Quat. Res.* **24**, 1 (1985).
9. G. O. Seltzer, *Quat. Res.* **41**, 154 (1994).
10. G. Seltzer, D. Rodbell, S. Burns, *Geology* **28**, 35 (2000).
11. G. O. Seltzer *et al.*, *Science* **296**, 1685 (2002).
12. P. A. Baker *et al.*, *Science* **291**, 640 (2001).
13. P. M. Tapia, S. C. Fritz, P. A. Baker, G. O. Seltzer, R. B. Dunbar, *Palaeogeogr. Palaeoclimatol. Palaeoecol.* **194**, 139 (2003).
14. G. M. Paduano, M. B. Bush, P. A. Baker, S. C. Fritz, G. O. Seltzer, *Palaeogeogr. Palaeoclimatol. Palaeoecol.* **194**, 259 (2003).
15. R. Garreaud, M. Vuille, A. C. Clement, *Palaeogeogr. Palaeoclimatol. Palaeoecol.* **194**, 5 (2003).
16. J. C. Gosse, F. M. Phillips, *Quat. Sci. Rev.* **20**, 1475 (2001).
17. Details of materials, methods, ^{10}Be data, and calculations are available as supporting material on *Science* Online.
18. J. A. Smith, D. L. Farber, R. C. Finkel, G. O. Seltzer, D. T. Rodbell, *Geol. Soc. Am. Annu. Meeting Progr.* **34**, 131 (2002).
19. On the lowest lateral moraine (~3400 masl), the exposure ages of boulders of the same lithology as the adjacent bedrock (granite) are young (~3 to 12 ky B.P.), whereas those of erratic lithologies (schist/quartzite) are late glacial (~15 to 17 ky B.P.), suggesting a localized rockfall component of the boulder population. This was not noted at other sampling locations.

20. The presence of boulders with a span of exposure ages (~34 to 22 ky B.P.) on the LLGM moraines may mean that glacier termini remained close to their maxima for up to ~12,000 years or fluctuated, building composite moraines. It is also possible that younger ages represent the effects of boulder exhumation, movement, or differential boulder erosion.
21. R. Müller, thesis, University of Zürich (1985).
22. M. Stute *et al.*, *Science* **269**, 379 (1995).
23. D. W. Lea, D. K. Pak, H. J. Spero, *Science* **289**, 1719 (2000).
24. J. Oerlemans, in *Glacier Fluctuations and Climatic Change*, J. Oerlemans, Ed. (Kluwer Academic, Dordrecht, Netherlands, 1989), pp. 353–371.
25. D. H. Clark, M. M. Clark, A. R. Gillespie, *Quat. Res.* **41**, 139 (1994).
26. A. M. Johnson, in *World Survey of Climatology, Vol. 12*, W. Schwerdtfeger, Ed. (Elsevier, New York, 1976), pp. 147–218.
27. S. C. Fritz *et al.*, *Quat. Res.* **61**, 95 (2004).
28. P. A. Baker *et al.*, *Nature* **409**, 698 (2001).
29. J. Imbrie *et al.*, in *Milankovitch and Climate, Part I*, A. L. Berger, J. Imbrie, J. Hays, G. Kukla, B. Saltzman, Eds. (Reidel, Dordrecht, Netherlands, 1984), pp. 269–305.
30. L. A. Owen *et al.*, *Quat. Sci. Rev.*, in press.
31. G. D. Thackray, *Quat. Res.* **55**, 257 (2001).
32. T. V. Lowell, *Quat. Sci. Rev.* **14**, 85 (1995).
33. We acknowledge financial and/or material support from the National Geographic Society (grant 7188-02), Lawrence Livermore National Laboratory, the Geological Society of America, Union College, Syracuse University, and NSF (grant ATM-0081517). We are grateful to two anonymous reviewers whose comments and suggestions substantially improved the manuscript. We dedicate this report to the memory of our coauthor, colleague, and friend, Geoff Seltzer, who was an integral part of the project from beginning to end.

Supporting Online Material
www.sciencemag.org/cgi/content/full/308/5722/678/DC1
Materials and Methods
SOM Text
Figs. S1 and S2
Table S1
References

3 November 2004; accepted 25 February 2005
10.1126/science.1107075

Laboratory Earthquakes Along Inhomogeneous Faults: Directionality and Supershear

Kaiwen Xia,[1,2]* Ares J. Rosakis,[1]† Hiroo Kanamori,[2] James R. Rice[3]

We report on the experimental observation of spontaneously nucleated ruptures occurring on frictionally held bimaterial interfaces with small amounts of wave speed mismatch. Rupture is always found to be asymmetric bilateral. In one direction, rupture always propagates at the generalized Rayleigh wave speed, whereas in the opposite direction it is subshear or it transitions to supershear. The lack of a preferred rupture direction and the conditions leading to supershear are discussed in relation to existing theory and to the earthquake sequence in Parkfield, California, and in North Anatolia.

There is evidence for supershear rupture propagation during earthquakes (*1*–*6*), and the link between large earthquakes and the conditions leading to supershear has been established experimentally (*7*).

Although many of the physical aspects of dynamic rupture (including supershear) are recently becoming clearer in relation to homogeneous faults (i.e., faults separating the same material) (*7*–*13*), the behavior of spontaneously nucleated ruptures in inhomogeneous faults (i.e., separating materials with different wave speeds) is still experimentally unexplored except in (*14*). Because many large earthquakes rupture on faults separating rock masses with different wave speeds, the mechanics of sliding in bimaterial systems is relevant to seismology. Specifically, the questions of whether a preferred rupture direction exists (*11*), whether a unilateral or bilateral faulting dominates (*15*), and what the condition is for supershear rupture propagation are particularly relevant to fault dynamics. These questions are also relevant to hazard potentials of large earthquakes, because directionality and rupture speed control near-field ground motions.

According to analysis and numerics, there are two types of such steady, self-sustained pulses (*16*, *17*). One type corresponds to rupture growth in the direction of slip in the lower wave speed material of the system, and this direction is referred to as the positive direction (*10*, *11*). The rupture pulses belonging to this type are subshear and always propagate with a steady velocity $V = +C_{GR}$, the generalized Rayleigh (GR) wave speed of the system. In this work, we refer to such ruptures as positive GR ruptures and abbreviate them as +GR ruptures. The second type of self-sustained ruptures corresponds to propagation in the negative direction opposite to +GR ruptures (*17*, *18*). Such pulses are supershear and always propagate with a steady velocity that is slightly lower than the *P*-wave speed of the material with the lower wave speed ($V = -C_P^2$). In the present paper, we will abbreviate such ruptures as $-P_{SLOW}$ ruptures.

Our experiments examined the effect of material contrast on the rupture growth of spontaneously nucleated dynamic ruptures hosted by inhomogeneous, frictional interfaces. These interfaces are held together by static, far-field pressure-shear simulating natural tectonic loads. The experiments mimic natural earthquakes where bimaterial contrast between intact rock masses seldom exceeds 30% in shear wave speeds (*10*). The experimental setup is similar to that used in our previous study of rupture in homogeneous interfaces (*7*). This configuration has proven effective in producing accurate, full-field, and real-time information of generic rupture characteristics that can ultimately be related to the rupture behavior of natural fault systems.

A Homalite-100 [Homalite (Division of BIG, Incorporated), Wilmington, DE] plate (material 1, top) and a polycarbonate plate (material 2, bottom) are held together by far-field load, *P* (Fig. 1). The ratio of shear wave speeds in the materials, $C_S^1/C_S^2 = 1.25$, is chosen to be at the high end of the naturally occurring bimaterial range so that the interfacial phenomena of interest are observable in the experiments. The shear wave speeds (Fig. 1) are directly measured for each material by following the shear wave fronts with the use of high-speed photography and photoelasticity. Photoelasticity, being sensitive to maximum shear stress fields, is perfectly suited for measuring shear wave speeds and for scrutinizing shear-dominated rupture processes in brittle, transparent, and birefringent solids (*7*). The *P*-wave speeds were calculated by using measured values of Poisson's ratios ($\nu^1 = 0.35$, $\nu^2 = 0.38$) and by using the directly measured shear wave speeds. Plain strain values were used, because we are interested in processes that take place at short wavelengths near the front of the rupture. An independent measurement of the longitudinal wave (*P* wave) speeds in the plates using ultrasonic transducers has confirmed these calculated values to within 5%. GR waves for this bimaterial pair exist, and their speed is calculated to be $C_{GR} = 959$ m/s, a value which is close to the shear wave speed of polycarbonate.

The dynamic rupture is triggered by means of an exploding wire mechanism, which simulates a localized pressure release at the desired location of the simulated hypocenter (*7*). About 32 experiments featuring different angles, α (20°, 22.5°, and 25°), and far-field loading *P* (10, 13, and 18 MPa) were performed, and the rupture events were repeatedly visualized in intervals of 3 μs by a digital high-speed camera system used in conjunction with dynamic photoelasticity (*7*).

[1]Graduate Aeronautical Laboratories, California Institute of Technology (Caltech), Pasadena, CA 91125, USA. [2]Seismological Laboratory, Caltech, Pasadena, CA 91125, USA. [3]Division of Engineering and Applied Sciences and Department of Earth and Planetary Sciences, Harvard University, Cambridge, MA 02138, USA.

*Present address: Division of Engineering, Brown University, Box D, Providence, RI 02912, USA.
†To whom correspondence should be addressed. E-mail: rosakis@aero.caltech.edu